Antibacterial and antiviral *N*-halamine nanofibrous membranes with nanonet structure for bioprotective applications

Congcong Tian [a,b], Fan Wu [a,b], Wenling Jiao [a,b], Xiaoyan Liu [b], Xia Yin [a,b,c,**], Yang Si [a,b,c,*], Jianyong Yu [a,b,c], Bin Ding [a,b,c]

[a] *Key Laboratory of High-Performance Fibers and Products, Ministry of Education, Donghua University, Shanghai, 200051, China*
[b] *College of Textiles, Donghua University, Shanghai, 201620, China*
[c] *Innovation Center for Textile Science and Technology, Donghua University, Shanghai, 200051, China*

ABSTRACT

The recent outbreak of a coronavirus disease (COVID-19) has posed a great threat to public health and financial system. Most current masks used to prevent the spread of COVID-19 are typically absence of biocidal properties. We designed a novel polymer, polystyrene grafted by 5, 5-dimethylhydantoin and trimethylamine (PSDT), which possesses halamine site and cationic quaternary ammonia salt site. Furthermore, PSDT/PU nanofiber@net membranes (PSDT/PU NNMs) were obtained by electrospinning technology. Our strategy enables inherent N-halamine and quaternary ammonia salt (QAS) group to be covalently integrated into membranes, realizing the efficient and stable biocidal properties. Meanwhile, the introduction of nanonets endows electrospun membranes with prominent air filtration performance. The resulting membranes exhibit integrated properties of high interception of fine particles (96.7%) and low pressure drop (95.4 Pa). Besides, chlorinated PSDT/PU nanofiber@net membranes (with active chlorine content of 0.60 wt% and quaternary ammonia salt content of 2.20 wt%) exhibited superior bactericidal (>99.9999%) and virucidal (>99.999%) efficiency in a short time (2 min), which enables chlorinated PSDT/PU NNMs to be served as the filtration material by providing bacterial interception (99.77%) and contact killing against pathogens. The successful synthesis of PSDT/PU NNMs provide innovative insights for exploring filtration materials in a nanonet and biocidal form.

1. Introduction

The recent outbreak of a coronavirus disease (COVID-19) has posed a significant global public health threat, resulting in dramatic social and economic crisis [1]. As of November 2020, the World Health Organization has reported more than 50,000,000 infected people and 120,000 deaths globally. Coronavirus spread through micro-droplets in the exhaled air or oral secretions of coughs and sneezes from the infected individuals to non-infected others. World health organization regulations indicated that it was compulsory to utilize masks in the public [2,3]. Although the existing protective masks, such as 3M N95 dust masks, can provide highly effective protection for individuals, pathogens intercepted and captured on the surface possess the sustained infection activity, thus triggering cross-infection and post-infection [4,5]. Among the cases of COVID-19 from Zhongnan Hospital in Wuhan, the broken city of COVID-19, 41.3% of people were cross-infected in the hospital

[6]. It is a feasible strategy to incorporate biocidal agents such as silver nanoparticles, triclosan, copper oxide, iodine, titanium oxide into the material surfaces to prevent the cross infection [7–10]. However, these materials failed to kill bacteria and viruses efficiently and rapidly due to the weak power of biocides [11]. Therefore, more effective protective materials are needed to confront the threat of emerging infectious diseases.

Cyclic *N*-halamine, one of the most promising disinfectants, has shown favorable properties including ease to regeneration and highly efficient biocidal activity in a short time. It is worth noting that 5, 5-dimethylhydantoin *N*-halamine compounds can kill germs faster than other *N*-halamine compounds such as tetramethyl piperidine or melamine *N*-halamine compounds with the same chlorine content [12–17]. A great deal of research is concentrated on chemically incorporating 5, 5-dimethylhydantoin *N*-halamine compounds into textiles especially by employing liquid soakage technique followed by heating treatment

---

[18–21]. Worley S. D. group made 5, 5-dimethylhydantoin potassium salt graft onto the backbone of polymer. Afterwards, the cotton cloth was soaked in the synthesized polymer solution and further cured to bond the *N*-halamine precursor polymer covalently [22]. However, the halamine precursor compound was incapable of bonding with the textiles sufficiently, thus peeling off the textiles easily under harsh condition and leading the sudden decrease of biocidal activity [23–25]. Therefore, the difficulty lies in developing homogeneous, covalently integrated and stable protective materials with intrinsically biocidal efficacy.

Here, we synthesized a novel polymer PSDT by nucleophilic substitution reaction with the synthetic system composed of chloromethylated Polystyrene (CMPS), 5, 5-dimethylhydantoin and trimethylamine. Subsequently, PSDT/PU NNMs were obtained by electrospinning technology. The material exhibited the following integrated properties: (i) superior biocidal efficacy originating from the synergistic effect of *N*-halamine, QAS and nanonets, (ii) high filtration efficiency and low resistance owing to the existence of Voronoi-like nanonets.

2. Results and discussion

2.1. Design and biocidal functions of PSDT/PU NNMs

We designed PSDT/PU NNMs based on three criteria: (i) the *N*-halamine and QAS must be homogeneously and chemically integrated into polymers backbone, (ii) the electrospun membranes must possess characters of effectively biocidal efficacy, and (iii) the membrane must have the filtration performance of high efficiency and low resistance. The first two requirements were met by a readily available grafting reaction of polymer in organic solvents. To satisfy the last criteria, hybrid

PSDT/PU NNMs were prepared by electrospinning technology. What is noteworthy is that the introduction of quaternary ammonium salt had the following advantages: (i) increasing the chlorine content from 790 ppm to 6030 ppm because enhanced hydrophilicity of nanofiber materials facilitated the grafting of *N*-halamine ; (ii) changing conductivity of the polymer solution, thus enabling the polymer to be drawn into multi-level nanometer structure containing nanofiber with a diameter of 199 ± 55 nm and nanonets with a diameter of 38 ± 7 nm; (iii) prolong the service life of the materials as a supplementary and stable biocidal group. Plentiful previous researches showed that the antimicrobial material containing *N*-halamine or quaternary ammonia salt group showed no cytotoxicity [26–28].

The preparation and biocidal procedure of the PSDT/PU NNMs were presented in Fig. 1. Polystyrene (PS) was chloromethylated firstly using 1, 4-bis(chloromethoxy) butane. Subsequently a biocidal precursor, PSDT, was then synthesized by nucleophilic substitution reaction with the synthetic system composed of CMPS, 5, 5-dimethylhydantoin (DMH) and trimethylamine (TMA). PSDT/PU NNMs were obtained using electrospinning technology. In the process, tiny charged droplets were sprayed and rapidly evolved into two-dimensional due to the phase separation. Meanwhile, the jets were drawn into typical nanofibers as a scaffold [29–31]. The obtained membranes with the PSDT/PU mass ratio of x : y were denoted as PSDT/PU NNMs-x:y. For comparison, PS/PU nanofiber membranes (PS/PU NMs) were prepared by a common electrospinning method.

It is widely reported that the *N*-halamine precursor compounds can possess highly effective biocidal and recyclable activity by halogenating [32,33]. The post-halogenation method is easier than the pre-halogenation method in electrospinning and the post-processing process, such as collection and storage [34]. As demonstrated in
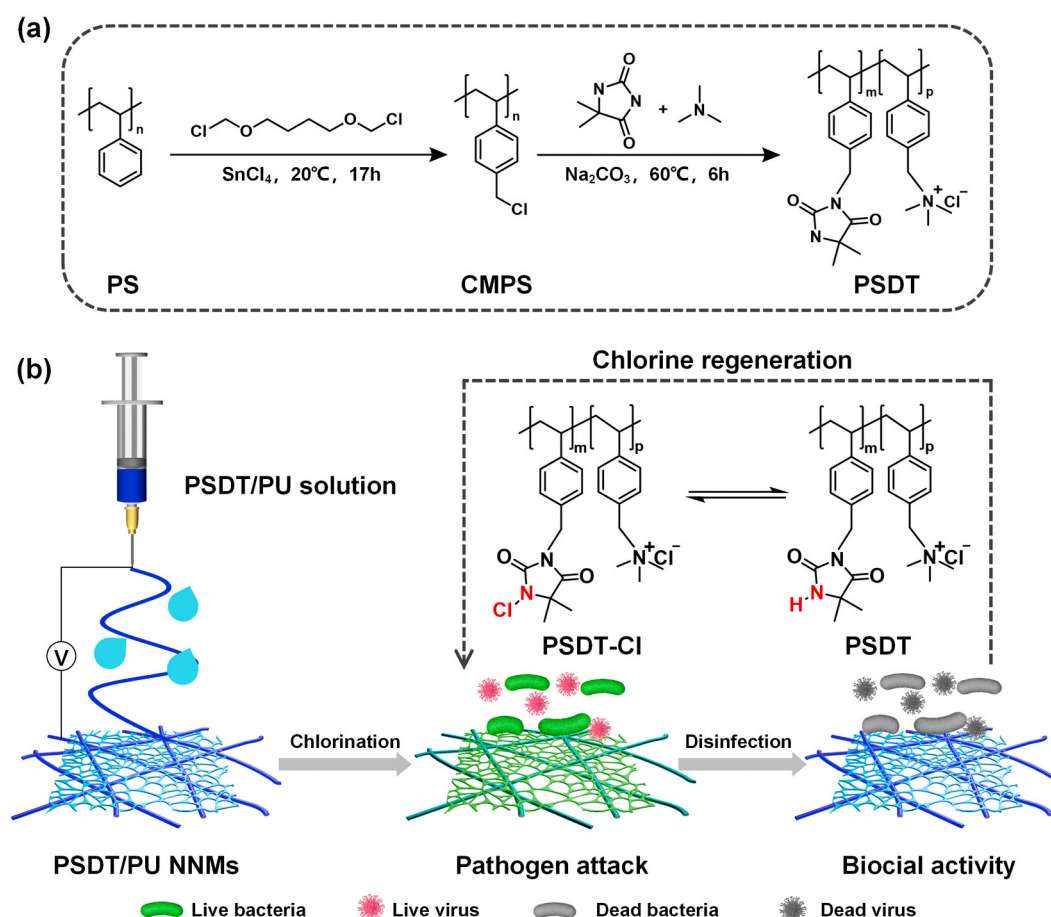

Fig. 1. (a) Synthesis pathway of CMPS and PSDT. (b) Schematic illustration of preparation and biocidal procedure of PSDT/PU NNMs.

Figure. l, N–H groups of PSDT could turn into biocidal N–Cl moieties by chlorinating, thus constructing chlorine-recyclable and quaternary ammonia PSDT/PU NNMs (PSDT/PU NNMs-Cl). Once pathogens were intercepted and in contact with the surface of the PSDT/PU NNMs-Cl, they were captured tightly by positively charged nitrogen of membranes due to the existence of QAS [35]. Subsequently, oxidized chlorine originated from the N–Cl moieties was transferred to appropriate receptors of pathogens to oxidize vital constituents for microorganisms' survival, like proteins or enzymes containing sulfhydryl group. Meanwhile, the N–Cl reverted to the precursor N–H. It was worth noting that *N*-halamine played a dominant and crucial role in killing pathogen because of the weakness of QAS biocidal activity. Afterwards, the biocidal N–Cl groups can be renewed by soaking or rising the materials with sodium hypochlorite solution [36,37].

2.2. Structural characterization and chlorine content optimization of PSDT

The chemical structures of PS, CMPS, PSDT, chlorinated PSDT (PSDT-Cl) were investigated by 1H Nuclear Magnetic Resonance (NMR), Fourier Transform Infrared Spectroscopy (FTIR) and X-ray Photoelectron Spectroscopy (XPS). CDCl$_3$ and DMSO-d6 were used as solvents respectively to gather the 1H NMR spectra of CMPS and PSDT shown in Fig. 2a. The signal observed at 4.49 ppm in 1H NMR spectra of CMPS was ascribed to protons in the chloromethyl group. By calculating the peak areas at 4.49 ppm and 1.84 ppm ascribed to protons attached to the first position carbon atom in backbones of polystyrene, the chlorine content of CMPS can be obtained as 2.15% [38]. In 1H NMR spectra of PSDT, the signal observed at 4.47 ppm and 2.95 ppm was ascribed to protons in the chloromethyl group and three methyl groups of quaternary ammonia salt respectively [39]. From peak areas at 4.47 ppm and 2.95 ppm of 1H NMR spectra of PSDT and the chlorine content of CMPS, the content of quaternary ammonia salt group was obtained as 2.20%.

The FT-IR spectra of samples were shown in Fig. 2b. Compared with that of PS, C–Cl bending vibration of chloromethyl group at 1420 cm^{-1} was detected in the FT-IR spectra of CMPS. The peak centered at 1263

cm^{-1} was ascribed to the bending vibration of the C–H groups in the 1, 4-disubstituted benzene ring, which was strengthened after the 4th position on the benzene ring was substituted by chloromethyl group [40]. An infrared spectrum of PSDT showed distinct bands at 1715 and 1769 cm^{-1}, demonstrating the existence of the hydantoin moieties. The infrared spectrum of PSDT-Cl showed two bands of 1728 and 1790 cm^{-1} derived from monochlorinated hydantoin moieties [12].

The elemental compositions of CMPS, PSDT and PSDT-Cl were identified by XPS in Fig. 2c. To fully elucidate the chemical environment of N and Cl in the sample, N 1s and Cl 2p core-level spectra were shown in Fig. 2d and e respectively. In the high-resolution N 1s spectrum of PSDT, three peaks centered at 402.7, 402.1 and 400 eV were ascribed to -N<, N+ and N–H respectively. As for PSDT-Cl, three peaks centered at 402.4, 401.7 and 401 eV were ascribed to -N<, N+ and N–Cl. In the high-resolution Cl 2p spectrum of CMPS, two peaks centered at 201 and 199.4 eV were ascribed to C–Cl 2p1/2 and C–Cl 2p2/3. With regard to PSDT, two peaks centered at 197 and 198.6 eV were assigned to Cl-2p1/2 and Cl-2p2/3. The peaks at 202.5, 200.9, 197 and 198.6 eV were assigned to N–Cl 2p1/2, N–Cl 2p2/3, Cl- 2p1/2 and Cl-2p2/3 in Cl 2p spectrum of PSDT-Cl [41–44]. The mentioned characterization above demonstrated the success of grafting reaction and chlorination.

The chlorine content of PSDT-Cl directly reflected the grafting amount of *N*-halamine and pathogens killing performance [44]. Therefore, chlorine content of PSDT-Cl prepared by different feed ratio of DMH and TMA was investigated. Fig. 2f showed that PSDT-Cl possessed the highest chlorine content of 2195 ppm when the feed ratio of DMH and TMA was 5:5. With increased feed mass of TMA, enhanced chlorine content of PSDT-Cl might be attributed to the hydrophilicity of QAS, which made the chlorination reaction more sufficient [43]. However, when the feed ratio of DMH and TMA changes from 5:5 to 2:8, the proportion of DMH grafted on chloromethylated polystyrene decreased, thus leading to the decreased chlorination site and chlorine content. Afterwards, *N*-halamine precursor with the highest chlorine content was used to obtain PSDT/PU NNMs by electrospinning.
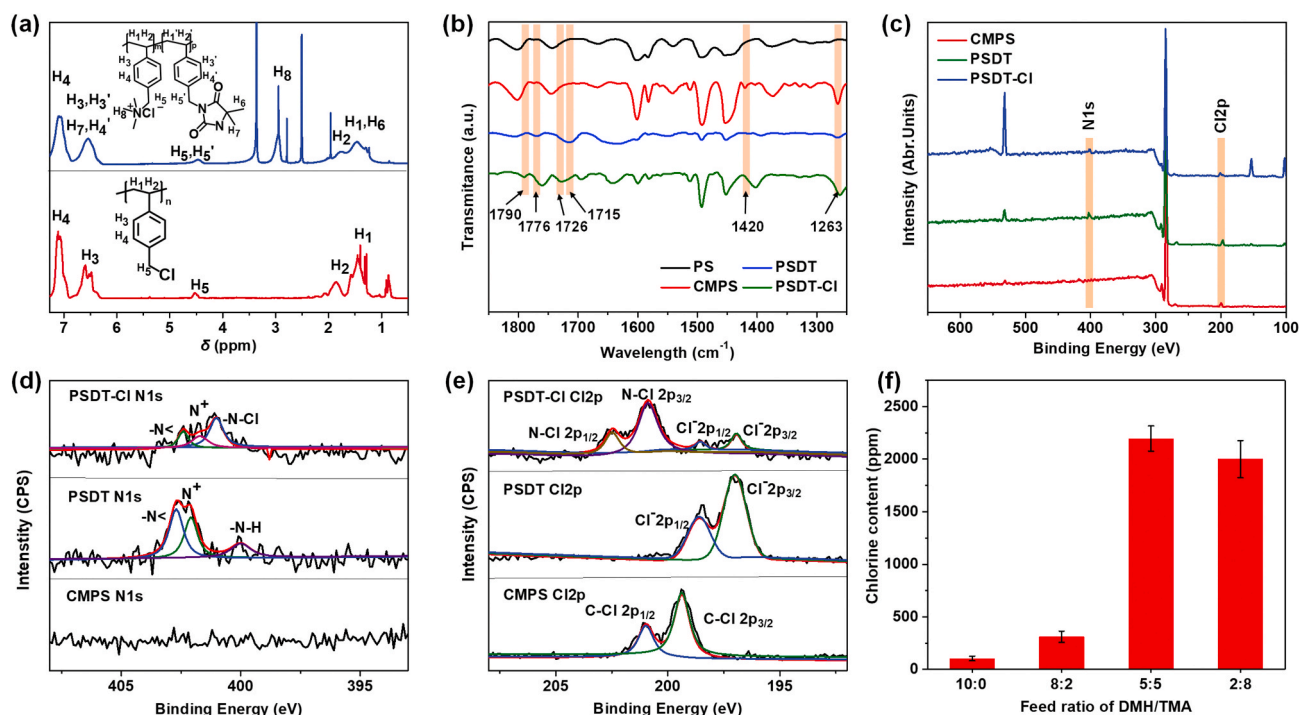

Fig. 2. (a) 1 H NMR spectra, (b) FT-IR spectra, (c) XPS spectra and XPS fitting curves of (d) N1s and (e) Cl 2p peak of CMPS, PSDT and PSDT-Cl. (f) Chlorine content of PSDT-Cl synthesized with different feed ratios of DMH and TMA.

2.3. Structure and filtration performance of PSDT/PU NNMs

Nanofibers and nanostructured networks have demonstrated great promise in constructing superior filter property due to their desirable attribute with reduced fiber diameters [45–48]. The effect of PU on the morphology of the Voronoi-like nanonets in the PSDT/PU NNMs was shown in Fig. 3a–c. With the mass ratio of PSDT and PU decreasing from 5:1 to 4:2, the material exhibited that the coverage rate of Voronoi-nets increased from 15% to 57%. The nanonets were more evenly distributed in the nanofiber scaffold, which is attributed to that PU component could decrease charge dissipation of charged fluid, thus causing more droplets to be ejected. However, with further mass ratio decreasing, nanonets tended to disappear and turned into the coverage rate of 0.3% on account that the reduced charge in Taylor cone liquid made charged liquid incapable of exceeding the droplet threshold to spay droplets [49]. The pore size and distribution of the PSDT/PU NFN were analyzed using a capillary flow porometer (CFP) in Fig. 3d. The pore size of PSDT/PU NNMs-5:1 and PSDT/PU NNMs-3:3 centrally distributed at 1.5 and 1.87 μm respectively. It was worth mentioning that the pore size of PSDT/PU NFN-4:2 concentrated in two peaks located at 0.34 and 0.96 μm due to the existence of Voronoi-like nanonet, which was also confirmed by the scanning electron microscope (SEM).

The filtration performances and mechanical properties of nanomaterials are critical in practical application [50,51]. Fig. 3e showed that PSDT/PU NNMs-4:2 exhibited the highest removal efficiency of 96.7%, the pressure drop of 95.4 Pa and favorable quality factor of 0.0359 Pa^{-1}, approximately three times larger than those of the commercial air filter materials [52]. Fig. 3f indicated that the tensile stress and elongation of PSDT/PU NNMs were improved with the increase of PU mass. PSDT/PU NNMs-4:2 exhibited over 2 and 6.45 times tensile stress and elongation respectively in comparison with PSDT/PU NNMs-5:1. Therefore, PSDT/PU NNMs-4:2 performing the optimal filtration performance were used to conduct further biocidal activity test.

2.4. Biocidal performance of PSDT/PU NNMs

Biocidal N–Cl moieties of the electrospun membranes were obtained by chlorinating N–H groups of PSDT. Fig. 4a showed the active chlorine contents of PSDT/PU NNMs-Cl during 10 chlorination/quenching

cycles. The stable and high chlorine content (>5000 ppm) of PSDT/PU NNMs-Cl could be ascribed to strong covalent bonding between hydantoin and PS backbones. *E. coliphage* D24291 was used to assess the antiviral performance of PSDT/PU NNMs-Cl (10 mg) with the active chlorine content of 0.60 wt% and quaternary ammonia salt content of 2.20 wt%. As shown in Fig. 4b, PSDT/PU NNMs-Cl showed 5 log PFU of *E. coliphage* killing within 2 min. The biocidal activity was dramatically better than previously reported virus-killing materials based on active chlorine [53].

The antibacterial performance of the materials with a mass of 10 mg was tested against *E. coli and S. aureus*. Fig. 4c–d manifested that PSDT/PU NNMs-Cl membranes (10 mg) could kill 6 log CFU of *E. coli and S. aureus* within 2 min, while there was almost no *E. coli and S. aureus* reduction on PS/PU NMs. It is worth noting that PSDT/PU NNMs could also reduce 5 log CFU of *E. coli and S. aureus* within 30min on account of the presence of QAS. The two germicidal experiments for *E. coli* (gram-negative bacteria) and *S. aureus* (gram-positive bacteria) proved excellent broad-spectrum germicidal performance of PSDT/PU NNMs-Cl.

To deeply understand the bacteria-killing mechanism of the PSDT/PU NNMs-Cl, morphology of *E. coli* and *S. aureus* was investigated by SEM. As demonstrated in Fig. 4e–f, PSDT/PU NNMs-Cl bore resemblance to the mechanism of commercial chlorine disinfectants like 84 disinfectant [54]. The antibacterial performance was further demonstrated by fluorescence-based experiments. Fig. 4g–h showed that there were almost no red fluorescence-labeled cells (dead *E. coli* and *S. aureus*) in the suspension of *E. coli* and *S. aureus* in contact with PS/PU-NMs. On the contrary, there were almost dead *E. coli* and *S. aureus* in the suspension of the *E. coli* in contact with PSDT/PU NNMs-Cl for 2 min, revealing the robust biocidal activity of PSDT/PU NNMs-Cl. Besides, bacterial filter efficiency (BFE) of PSDT/PU NNMs-Cl was investigated according to the standard of ASTM F2101-19. As Fig. 4i, BFE of PSDT/PU NNMs-Cl can be obtained as 99.77% by calculating the number of bacterial aerosol particles upstream and downstream.

3. Conclusion

In summary, we present unique strategy for the construction of intrinsically antibacterial and antiviral PSDT/PU NNMs through the combination of a novel polymer and electrospinning nanofibers@net membranes. Profiting from the synergy of *N*-halamine, ammonium salt,
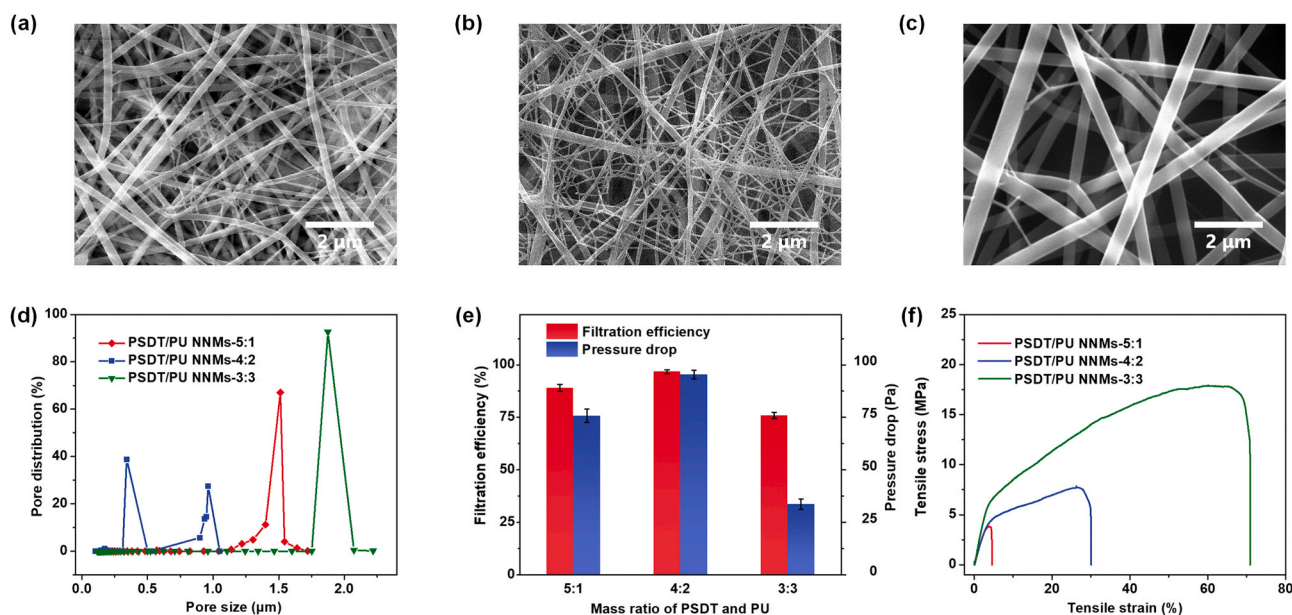

Fig. 3. SEM images of (a) PSDT/PU NNMs-5:1, (b)PSDT/PU NNMs-4:2 and (c) PSDT/PU NNMs-3:3. (d) Pore size distribution, (e) filtration performance and (f) mechanical properties of the PSDT/PU NNMs.
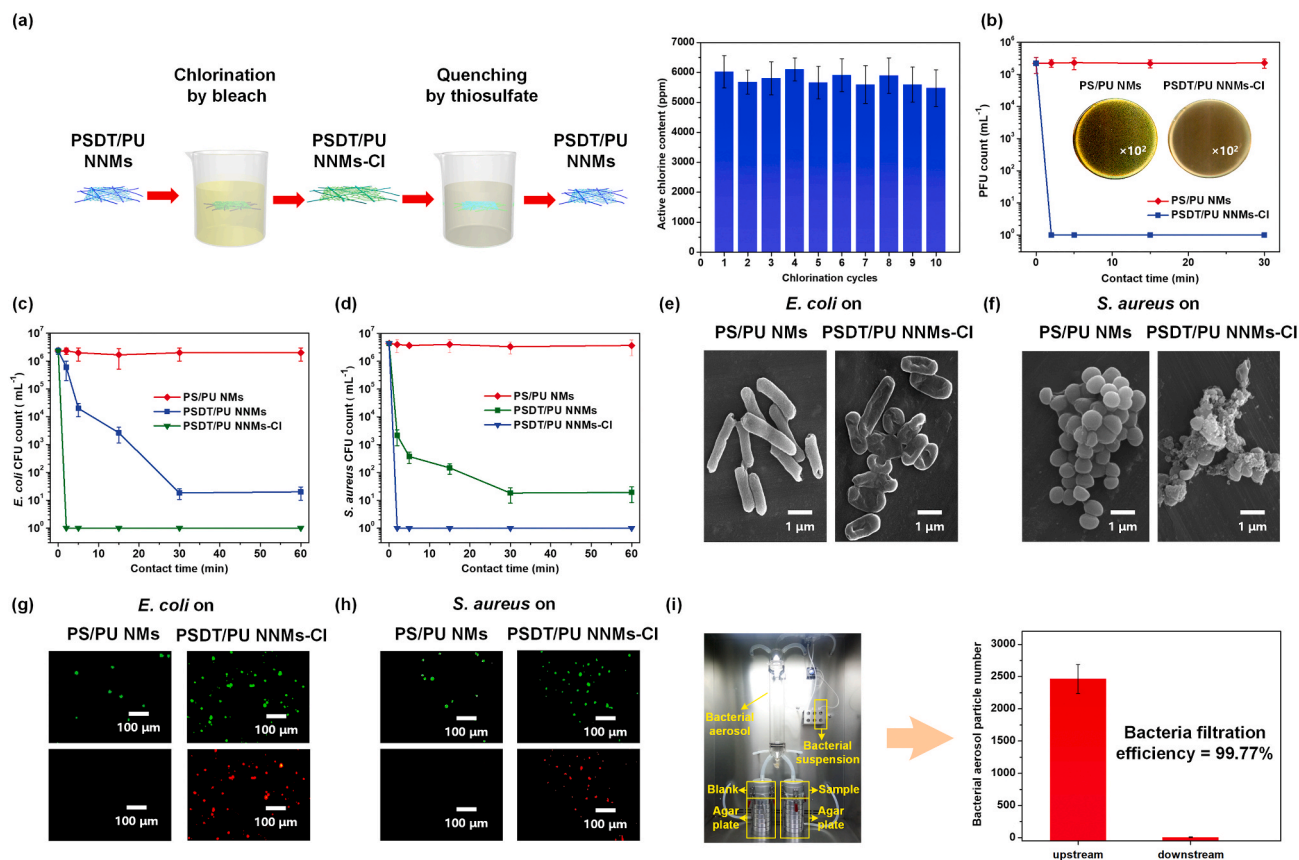
Fig. 4. (a) Ten cyclic chlorination tests. (b) Antiviral activity against *E. coliphage* D24291. Bactericidal activity against (c) *E. coli* and (d) *S. aureus*. SEM images of live/dead (e) *E. coli* and (f) *S. aureus* in contact with PS/PU NMs and PSDT/PU NNMs-Cl. Fluorescent images of live/dead (g) *E. coli* and (h) *S. aureus* in contact with PS/PU NMs and PSDT/PU NNMs-Cl. (i) Bacteria filtration efficiency of PSDT/PU NNMs-Cl.

high specific surface area, robust mechanical properties, PSDT/PU NNMs-Cl with the chlorine loading of 0.60 wt% and quaternary ammonia salt loading of 2.20 wt% can effectively reduce *E. coli* and *S. aureus* of 6 log CFU and *E. coliphage* D24291 of 5 log PFU within 2 min. In addition, due to the unique Voronoi-like nanonet structure, PSDT/PU NNMs possess high interception of fine particles (96.7%), low pressure drop (95.4 Pa) and high bacteria filtration efficiency (99.77%). These attributes enable PSDT/PU NNMs-Cl to be served as a reusable material for bioprotection by providing intercepting and killing functionality against pathogens, which contributes to preventing cross-infection and post-infection caused by typical masks. The successful preparation of the material also offers new thinking approaches for the development of other biocidal membranes in various applications, such as contaminated water treating and food packaging materials.

4. Experimental

4.1. Materials

Polystyrene (PS), carbon tetrachloride (CCl$_4$), *N*, *N*-Dimethylacetamide (DMAC), Tin chloride (SnCl$_4$), sodium carbonate (Na$_2$CO$_3$), 5,5-dimethylhydantoin (DMH), trimethylamine solution (TMA, 30 wt%) were bought from Aladdin Chemistry Co. Ltd., China. 1,4-bis(chloromethoxy) butane was supplied by Xi'an langene biological technology co., Ltd., China. Trimethylolpropane tris (2-methyl-1-aziridine propionate) (TTMA) was purchased by Shanghai Zealchem Co., Ltd., China. PU was bought from Huntsman Polyurethanes Co. Ltd., China. Propidium iodide, SYBR Green, Luria-Bertani (LB) broth, and LB agar were supplied by Sangon Biotech Co.,Ltd.,China.

4.2. Synthesis of PSDT

BCMB (17.1 mL) was dropwise added into the CCl$_4$ solution of PS (10.415 g) and SnCl$_4$ (5 mL). When the drip was over, the mixture was stirred for 17 h at 18 °C. Then the mixture treated by HCl (1 mol L^{-1}, 240 mL) was washed and filtered repeatedly with EtOH and Deionized water. Subsequently, the as-obtained CMPS (3 g), DMH, Na$_2$CO$_3$ and TMA were dissolved into DMAC (180 mL) and stirred for 6 h at 60 °C. Then PSDT powder was obtained by washing and filtering with NaCl solution (16.7 wt%) and Deionized water. PSDT-Cl powder was obtained when the mixture was dripped into NaClO solution (2.5 wt%), stirred for 1 h and washed with deionized water.

4.3. Preparation of PSDT/PU NNMs

The electrospinning solution was obtained by dissolving PSDT, PU and TTMA in DMAC. The concentrations of PSDT and TTMA were optimized as 12.5 wt% and 10 wt%, respectively. The as-prepared solutions were powered by direct voltage of 40 kV, pumped out at the feed rate of 1 mL h^{-1} and collected on a metallic cylinder at the environment of 23 ± 2 °C and 40 ± 5%RH. Afterwards, PSDT/PU NNMs were dried at 60 °C for 30 min with the presence of acetic acid for cross-linking.

4.4. Filtration performance measure

The coverage rate of the Voronoi-like nanonets was obtained using Adobe Photoshop CS6. The pore size and distribution of materials were investigated using CFP (CFP-1100AI, Porous Materials Inc., American). Filtration performance of PSDT/PU NNMs were evaluated by using TSI 8130 automatic filter tester (TSI Inc.).

4.5. Chlorination and biocidal test

The PSDT/PU NNMs were sufficiently chlorinated by NaClO solution (2.5 wt%) for 1 h and completely quenched with superfluous thiosulfate. After a certain number of cycles, active chlorine content was measured by iodometric titration method.

The biocidal test was performed against *E. coli* (ATCC 25922), *S. aureus* (ATCC 25923) and *Escherichia coliphages* (SHBCC D24291) according to the absorption method of ISO 20743-2013 and ISO 18184-2019. The morphology of bacterium was investigated by SEM (VEGA 3, TESCAN Ltd, Czech). Fluorescence observation was conducted using microscope (Leica DMi8).

4.6. Characterization

The chemical structure of the product was characterized by NMR (AVANCE400, Bruker, Germany), FTIR (Thermo Scientific Nicolet is10, USA) and XPS (Escalab 250Xi, United States). The mechanical performance of the membranes was evaluated using a tensile tester (XQ-1C, China). The bacterial filtration efficiency was evaluated by Bacteria filtration efficiency tester (G299, Qinsun Instruments Co., China).

CRediT authorship contribution statement

Congcong Tian: Investigation, Writing - original draft. **Fan Wu:** Investigation. **Wenling Jiao:** Writing - review & editing. **Xiaoyan Liu:** Formal analysis. **Xia Yin:** Validation. **Yang Si:** Conceptualization, Methodology, Project administration. **Jianyong Yu:** Conceptualization, Methodology, Project administration. **Bin Ding:** Conceptualization, Methodology, Project administration.

Declaration of competing interest

The authors declare that they have no known competing financial interests or personal relationships that could have appeared to influence the work reported in this paper.

Acknowledgements

Appendix A. Supplementary data

Supplementary data to this article can be found online at https://doi.org/10.1016/j.coco.2021.100668.

References

[1] D. Lu, Z. Huang, J. Luo, X. Zhang, S. Sha, Primary concentration - the critical step in implementing the wastewater based epidemiology for the COVID-19 pandemic: a mini-review, Sci. Total Environ. 747 (2020) 141245.

[2] E. Atangana, A. Atangana, Facemasks simple but powerful weapons to protect against COVID-19 spread: can they have sides effect? Results Phys. 19 (2020) 103425.

[3] Y. Wibisono, C.R. Fadila, S. Saiful, M.R. Bilad, Facile approaches of polymeric face masks reuse and reinforcements for micro-aerosol droplets and viruses filtration: a review, Polymers 12 (2020), 12112516.

[4] Y. Si, Z. Zhang, W. Wu, Q. Fu, K. Huang, N. Nitin, B. Ding, G. Sun, Daylight-driven rechargeable antibacterial and antiviral nanofibrous membranes for bioprotective applications, Sci. Adv. 4 (2018), eaar5931.

[5] K. O'Dowd, K.M. Nair, P. Forouzandeh, S. Mathew, J. Grant, R. Moran, J. Bartlett, J. Bird, S.C. Pillai, Face masks and respirators in the fight against the COVID-19 pandemic: a review of current materials, advances and future perspectives, Materials 13 (2020) 3363.

[6] D. Wang, B. Hu, C. Hu, F. Zhu, X. Liu, J. Zhang, B. Wang, H. Xiang, Z. Cheng, Y. Xiong, Y. Zhao, Y. Li, X. Wang, Z. Peng, Clinical characteristics of 138 hospitalized patients with 2019 novel coronavirus-infected pneumonia in Wuhan, China, JAMA, J. Am. Med. Assoc. 323 (2020) 1061–1069.

[7] Y. Li, P. Leung, L. Yao, Q.W. Song, E. Newton, Antimicrobial effect of surgical masks coated with nanoparticles, J. Hosp. Infect. 62 (2006) 58–63.

[8] G. Borkow, S.S. Zhou, T. Page, J. Gabbay, A novel anti-influenza copper oxide containing respiratory face mask, PLoS One 5 (2010), e11295.

[9] S. Ratnesar-Shumate, C.Y. Wu, J. Wander, D. Lundgren, S. Farrah, J.H. Lee, P. Wanakule, M. Blackburn, M.F. Lan, Evaluation of physical capture efficiency and disinfection capability of an iodinated biocidal filter medium, Aerosol Air Qual. Res. 8 (2008) 1–18.

[10] J.H. Lee, C.Y. Wu, K.M. Wysocki, S. Farrah, J. Wander, Efficacy of iodine-treated biocidal filter media against bacterial spore aerosols, J. Appl. Microbiol. 105 (2008) 1318–1326.

[11] Y. Si, A. Cossu, N. Nitin, Y. Ma, C. Zhao, B.s. Chiou, T. Cao, D. Wang, G. Sun, Mechanically robust and transparent *N*-halamine grafted PVA-co-PE films with renewable antimicrobial activity, Macromol. Biosci. 17 (2017) 1600304.

[12] Y. Chen, S.D. Worley, T.S. Huang, J. Weese, J. Kim, C.I. Wei, J.F. Williams, Biocidal polystyrene beads. IV. functionalized methylated polystyrene, J. Appl. Polym. Sci. 92 (2004) 368–372.

[13] A. Dong, Y.J. Wang, Y. Gao, T. Gao, G. Gao, Chemical insights into antibacterial *N*-halamines, Chem. Rev. 117 (2017) 4806–4862.

[14] X. Sun, Z. Cao, N. Porteous, Y. Sun, Amine, melamine, and amide *N*-halamines as antimicrobial additives for polymers, Ind. Eng. Chem. Res. 49 (2010) 11206–11213.

[15] R. Bai, J. Kang, O. Simalou, W. Liu, H. Ren, T. Gao, Y. Gao, W. Chen, A. Dong, R. Jia, Novel N-Br bond-containing *N*-halamine nanofibers with antibacterial activities, ACS Biomater. Sci. Eng. 4 (2018) 2193–2202.

[16] R. Bai, Q. Zhang, L. Li, P. Li, Y.-J. Wang, O. Simalou, Y. Zhang, G. Gao, A. Dong, *N*-halamine-containing electrospun fibers kill bacteria via a contact/release co-determined antibacterial pathway, ACS Appl. Mater. Interfaces 8 (2016) 31530–31540.

[17] F. Wang, L. Huang, P. Zhang, Y. Si, J. Yu, B. Ding, Antibacterial *N*-halamine fibrous materials, Compos. Commun. 22 (2020) 100487.

[18] Z. Jiang, K. Ma, J. Du, R. Li, X. Ren, T.S. Huang, Synthesis of novel reactive *N*-halamine precursors and application in antimicrobial cellulose, Appl. Surf. Sci. 288 (2014) 518–523.

[19] K. Ma, Z. Xie, Q. Jiang, J. Li, R. Li, X. Ren, T.S. Huang, K.Q. Zhang, Cytocompatible and regenerable antimicrobial cellulose modified by *N*-halamine triazine ring, J. Appl. Polym. Sci. 131 (2014) 40627.

[20] B. Zhang, Y. Jiao, Z. Kang, K. Ma, X. Ren, J. Liang, Durable antimicrobial cotton fabrics containing stable quaternarized *N*-halamine groups, Cellulose 20 (2013) 3067–3077.

[21] R. Li, P. Hu, X. Ren, S.D. Worley, T.S. Huang, Antimicrobial *N*-halamine modified chitosan films, Carbohydr. Polym. 92 (2013) 534–539.

[22] I. Cerkez, H.B. Kocer, S.D. Worley, R.M. Broughton, T.S. Huang, Epoxide tethering of polymeric *N*-halamine moieties, Cellulose 19 (2012) 959–966.

[23] C. Liu, H. Shan, X. Chen, Y. Si, X. Yin, J. Yu, B. Ding, Novel inorganic-based *N*-halamine nanofibrous membranes as highly effective antibacterial agent for water disinfection, ACS Appl. Mater. Interfaces 10 (2018) 44209–44215.

[24] S. Zhang, B. Demir, X. Ren, S.D. Worley, R.M. Broughton, T.S. Huang, Synthesis of antibacterial *N*-halamine acryl acid copolymers and their application onto cotton, J. Appl. Polym. Sci. 136 (2019) 47426.

[25] T. Mu, N. Pan, Y. Wang, X. Ren, T.S. Huang, Antibacterial coating of cellulose by iso-bifunctional reactive *N*-halamine with the dyeing process of reactive dye, Fibers Polym. 19 (2018) 2284–2289.

[26] Y. Liu, M.Y. Qiao, C.H. Lv, X.H. Ren, G. Buschle-Diller, T.S. Huang, *N*-halamine polyelectrolytes used for preparation of antibacterial polypropylene nonwoven fabrics and study on their basal cytotoxicity and mutagenicity, Int. J. Polym. Mater. Polym. Biomat. 69 (2020) 971–978.

[27] Y.X. Zheng, N.Y. Pan, Y. Liu, X.H. Ren, Novel porous chitosan/*N*-halamine structure with efficient antibacterial and hemostatic properties, Carbohydr, Polym 253 (2021) 117205.

[28] S. Lan, Y.N. Lu, J.H. Zhang, Y.A. Guo, C. Li, S. Zhao, X.L. Sheng, A. Dong, Electrospun sesbania gum-based polymeric *N*-halamines for antibacterial applications, Polymers 11 (2019) 1117.

[29] S. Zhang, H. Liu, N. Tang, N. Ali, J. Yu, B. Ding, Highly efficient, transparent, and multifunctional air filters using self-assembled 2D nanoarchitectured fibrous networks, ACS Nano 13 (2019) 13501–13512.

[30] S. Zhang, H. Liu, N. Tang, J. Ge, J. Yu, B. Ding, Direct electronetting of high-performance membranes based on self-assembled 2D nanoarchitectured networks, Nat. Commun. 10 (2019) 1458.

[31] H. Liu, L. Liu, J. Yu, X. Yin, B. Ding, High-efficiency and super-breathable air filters based on biomimetic ultrathin nanofiber networks, Compos. Commun. 22 (2020) 100493.

[32] M. Natan, O. Gutman, R. Lavi, S. Margel, E. Banin, Killing mechanism of stable *N*-halamine cross-linked polymethacrylamide nanoparticles that selectively target bacteria, ACS Nano 9 (2015) 1175–1188.

[33] M. Liu, F. Wang, M. Liang, Y. Si, J. Yu, B. Ding, In situ green synthesis of rechargeable antibacterial *N*-halamine grafted poly(vinyl alcohol) nanofibrous membranes for food packaging applications, Compos. Commun. 17 (2020) 147–153.

[34] H. Ren, Y. Du, Y. Su, Y. Guo, Z. Zhu, A. Dong, A review on recent achievements and current challenges in antibacterial electrospun *N*-halamines, Colloid Interface Sci. Commun. 24 (2018) 24–34.

[35] Y. Chen, C. Feng, Q. Zhang, M. Luo, J. Xu, Q. Han, Engineering of antibacterial/recyclable difunctional nanoparticles via synergism of quaternary ammonia salt site and *N*-halamine sites on magnetic surface, Colloids Surf. B Biointerfaces 187 (2020) 110642.

[36] O. Gutman, M. Natan, E. Banin, S. Margel, Characterization and antibacterial properties of *N*-halamine-derivatized cross-linked polymethacrylamide nanoparticles, Biomaterials 35 (2014) 5079–5087.

[37] A. Dong, S. Lan, J. Huang, T. Wang, T. Zhao, L. Xiao, W. Wang, X. Zheng, F. Liu, G. Gao, Y. Chen, Modifying Fe$_3$O$_4$-functionalized nanoparticles with *N*-halamine and their magnetic/antibacterial properties, ACS Appl. Mater. Interfaces 3 (2011) 4228–4235.

[38] D. Xu, B. Gao, P. Chen, Preparation and characterization of polystyrene containing bidentate schiff base ligand on side chain and preliminary exploration of fluorescence emission property of its Eu(III) complexes, J. Biol. Chem. 32 (2015) 183–191.

[39] J. Pan, S. Lu, Y. Li, A. Huang, L. Zhuang, J. Lu, High-performance alkaline polymer electrolyte for fuel cell applications, Adv. Funct. Mater. 20 (2010) 312–319.

[40] Y. Shen, Y. Yang, B. Gao, Y. Zhu, Synthesis of linear chloromethylated polystyrene with 1,4-bis(chloromethoxyl) butane as chloromethylation reagent, Acta Polym. Sin. (2007) 559–565.

[41] C. Yao, X. Li, K.G. Neoh, Z. Shi, E.T. Kang, Surface modification and antibacterial activity of electrospun polyurethane fibrous membranes with quaternary ammonium moieties, J. Membr. Sci. 320 (2008) 259–267.

[42] F. Wang, J. Dai, L. Huang, Y. Si, J. Yu, B. Ding, Biomimetic and superelastic silica nanofibrous aerogels with rechargeable bactericidal function for antifouling water disinfection, ACS Nano 14 (2020) 8975–8984.

[43] Z. Jie, B. Zhang, L. Zhao, X. Yan, J. Liang, Regenerable antimicrobial silica gel with quaternarized *N*-halamine, J. Mater. Sci. 49 (2014) 3391–3399.

[44] Y. Si, J. Li, C. Zhao, Y. Deng, Y. Ma, D. Wang, G. Sun, Biocidal and rechargeable *N*-halamine nanofibrous membranes for highly efficient water disinfection, ACS Biomater. Sci. Eng. 3 (2017) 854–862.

[45] Y. Si, J. Yu, X. Tang, J. Ge, B. Ding, Ultralight nanofibre-assembled cellular aerogels with superelasticity and multifunctionality, Nat. Commun. 5 (2014) 5802.

[46] Q. Fu, Y. Si, C. Duan, Z. Yan, L. Liu, J. Yu, B. Ding, Highly Carboxylated, Cellular Structured, and underwater superelastic nanofibrous aerogels for efficient protein separation, Adv. Funct. Mater. 29 (2019) 1808234.

[47] G. Zhou, X. An, C. Zhou, Y. Wu, Y. Miao, T. Liu, Highly porous electroactive polyimide-based nanofibrous composite anode for all-organic aqueous ammonium dual-ion batteries, Compos. Commun. 22 (2020) 100519.

[48] H. Gu, Y. Huang, L. Zuo, W. Fan, T. Liu, Graphene sheets wrapped carbon nanofibers as a highly conductive three-dimensional framework for perpendicularly anchoring of MoS$_2$: advanced electrocatalysts for hydrogen evolution reaction, Compos. Commun. 219 (2016) 604–613.

[49] H. Liu, S. Zhang, L. Liu, J. Yu, B. Ding, High-performance PM0.3 air filters using self-polarized electret nanofiber/nets, Adv. Funct. Mater. 30 (2020), 1909554.

[50] U.Y. Karatepe, T. Ozdemir, Improving mechanical and antibacterial properties of PMMA via polyblend electrospinning with silk fibroin and polyethyleneimine towards dental applications, Bioact. Mater. 5 (2020) 510–515.

[51] X. Zhao, F. Yang, Z. Wang, P. Ma, W. Dong, H. Hou, W. Fan, T. Liu, Mechanically strong and thermally insulating polyimide aerogels by homogeneity reinforcement of electrospun nanofibers, Compos. Commun. 182 (2020) 107624.

[52] S. Lee, A.R. Cho, D. Park, J.K. Kim, K.S. Han, I.J. Yoon, M.H. Lee, J. Nah, Reusable polybenzimidazole nanofiber membrane filter for highly breathable PM2.5 dust proof mask, ACS Appl. Mater. Interfaces 11 (2019) 2750–2757.

[53] J. Sun, Y. Sun, Acyclic *N*-halamine-based fibrous materials: preparation, characterization, and biocidal functions, J. Polym. Sci., Polym. Chem. Ed. 44 (2006) 3588–3600.

[54] W.B. Rauen, A. Angeloudis, R.A. Falconer, Appraisal of chlorine contact tank modelling practices, Water Res. 46 (2012) 5834–5847.